Guided Search to Self-Healing in Semiconductors

Alexandre Py-renaudie, Yahel Soffer, Pallavi Singh, Sujit Kumar, Davide R Ceratti, Yuval Mualem, Irit Rosenhek-Goldian, Dan Oron, Sidney R Cohen, Philip Schulz, et al.

ADVANCED FUNCTIONAL MATERIALS
www.afm-journal.de

Guided Search to Self-Healing in Semiconductors

*Alexandre Py-Renaudie, Yahel Soffer, Pallavi Singh, Sujit Kumar, Davide R. Ceratti, Yuval Mualem, Irit Rosenhek-Goldian, Dan Oron, Sidney R. Cohen, Philip Schulz, David Cahen, and Jean-François Guillemoles**

Self-healing (SH) of (opto)electronic material damage can have a huge impact on resource sustainability. The rising interest in halide perovskite (HaP) compounds over the past decade is due to their excellent semiconducting properties for crystals and films, even if made by low-temperature solution-based processing. Direct proof of self-healing in Pb-based HaPs is demonstrated through photoluminescence recovery from photodamage, fracture healing and their use as high-energy radiation and particle detectors. Here, the question of how to find additional semiconducting materials exhibiting SH, in particular lead-free ones is addressed. Applying a data-mining approach to identify semiconductors with favorable mechanical and thermal properties, for which Pb HaPs are clear outliers, it is found that the $Cs_2Au^{I}Au^{III}X_6$, (X = I, Br, Cl) family, which is synthesized and tested for SH. This is the first demonstration of self-healing of Pb-free inorganic HaP thin films, by photoluminescence recovery.

1. Introduction

In recent years, halide perovskite (HaP) research has gained impressive momentum, especially, but not only, for solar cell research. This is mainly due to the high performances obtained from devices, based on Pb-HaP thin films, deposited via solution processes, the best of which have shown over 25.7% power solar to electrical power conversion efficiencies[1] as well as an increase in the stabilities of these devices.[2] Fundamental studies demonstrated that these HaPs display a high degree of dynamic structural disorder[3] combined with optoelectronic properties usually associated with highly crystalline semiconductors, such as long carrier lifetimes.[4] In the case of HaPs, defects either do not significantly affect properties such as carrier mobility or recombination rates in what is known as the defect tolerant (DT) model,[5,6] or the material reconstitutes in a self-healing (SH) process.[7] SH was already observed in a few semiconductors such as CIGS,[8] Si:Li[9] and (Cd,Hg)Te:Ag,[10,11] where the process was ascribed to relatively fast diffusion at operating temperatures, of Cu, Li or Ag, respectively. While in the case of lead HaPs SH likely has a different mechanism, a subject still being studied, it can be identified through photoluminescence, PL, recovery over time after damage by laser irradiation within the material or near and at its surface, as reported by Ceratti et al.[12,13] This experimental method is well established in life sciences where it is commonly referred to as FRAP, Fluorescence Recovery After Photobleaching.

While the proposed defect tolerance, i.e., the optoelectronic inactivity of existent defects, of Pb-HaPs awaits support by experimental data and a theoretical description which fully considers the effect of anharmonicity or dynamic disorder,[7,14] the experimental evidence for SH from photoluminescence recovery[12] and crack healing is clear.[15,16] We note that it is attractive to invoke ion mobility as a primary cause for this behavior, but to date there is no consistent model. The small free energies and activation energies for the formation of Pb-HaPs from their binaries, have been invoked as enabling agents for SH,[7] but the fundamental cause is likely the dynamics of the lattice and its strong anharmonicity.[17,18] These can be probed experimentally and are reflected in the relatively low elastic moduli of lead HaPs[18,19] as well as in their thermal properties.[20]

All in all, it is difficult to clearly associate self-healing in lead HaPs with one unique materials property and at this point we also do not yet have a figure of merit, encompassing values of several properties to deduce SH ability of a material from readily

A. Py-Renaudie, D. R. Ceratti, P. Schulz, J.-F. Guillemoles
CNRS, Ecole Polytechnique, ENSCP
Institut Photovoltaïque d'Île de France (IPVF)
UMR 9006, Palaiseau 91120, France
E-mail: jf.guillemoles@cnrs.fr

Y. Soffer
Department of Physics of Complex Systems
Weizmann Institute of Science
Rehovot 7610001, Israel

P. Singh, S. Kumar, Y. Mualem, D. Oron, D. Cahen
Department of Molecular Chemistry and Materials Science
Weizmann Institute of Science
Rehovot 7610001, Israel

I. Rosenhek-Goldian, S. R. Cohen
Department of Chemical Research Support Israel
Weizmann Institute of Science
Rehovot 7610001, Israel

The ORCID identification number(s) for the author(s) of this article can be found under https://doi.org/10.1002/adfm.202309107

DOI: 10.1002/adfm.202309107

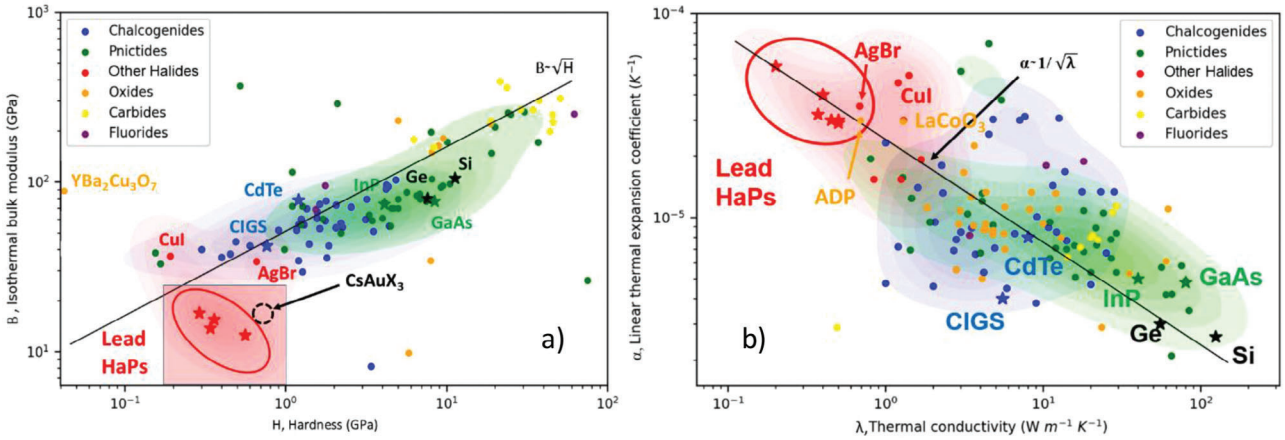

Figure 1. Plots of a) Isothermal bulk modulus versus hardness for semi-conductors and insulators and b) Linear thermal expansion coefficient versus thermal conductivity; dots are data taken from the MPDS database. Stars represent compounds of reference (for halides, including Pb-HaPs such as $MAPbI_3$, $CsPbI_3$, $MAPbBr_3$, ...). Each color refers to a specific anion group. Si and Ge are labeled in black.

measurable physical quantities. This situation impedes or even prevents any alternative to empirical searching for other candidate materials that self-heal. Here we show how to overcome this hurdle, at least partially, with data-mining.

Our starting hypotheses are that.

1) there exist some material properties that are markers of self-healing.
2) materials that display SH share some common behavior linked to material properties.

Thus, we looked for material properties of lead HaPs that stand out from the majority of a large sampling of known semiconductors. Upon identifying such properties, we then look for materials with relevant property values in the same range as Pb-HaPs. We then test such materials for self-healing using FRAP. Our method to infer the likelihood that a given semiconductor exhibits self-healing is based on a data-mining approach with a focus on mechanical and thermal properties of semiconductors, in view of the above-mentioned understanding of SH in Pb-HaPs.

Using this approach, we identified a known family of compounds ($Cs_2Au^{I}Au^{III}X_6$, with X = I, Br, Cl) and observed self-healing in two of those, which we evidenced by FRAP.

2. Results

The Ashby diagrams obtained from data-mining provide us with gradient maps that act as a guide to the eye for the area of high concentrations of data points for each family of compounds with respect to their anion, e.g. halides, oxides. Strictly speaking fluorides should be included in halides. Similarly, oxides are formally also chalcogenides. However, materials related to either of these anions do not follow the trend of the rest of the families. Moreover, oxides are over-represented in the thermal diagrams. For these reasons, oxides and fluorides are labeled distinctly in **Figure 1**. Similar diagrams were studied by classifying the compounds with respect to their cations but no obvious trend emerged from these diagrams, as can be seen in Figures S2 and S3 (Supporting Information).

We limited the data considered to those acquired close to room temperature. This reduces the volume of data, but helps avoid the pitfall of temperature dependence of certain properties (for instance thermal conductivity). Another obvious limitation is the absence of organic or even hybrid materials from the MPDS database. We added data for hybrid organic-inorganic HaPs wherever those were available from the peer-reviewed literature. The database was supplemented by our literature search for one or more properties of specific compounds when deemed necessary.

Among the 17 investigated properties, we could identify two property pairs where Pb-HaPs are clear outliers compared to the other semiconductors present in our database. These property pairs are:

1) thermal conductivity and linear thermal expansion coefficient.
2) isothermal bulk modulus and hardness.

The results are presented in Figure 1.

The hardness measurements reported in the Materials Project database contain microhardness as well as nanohardness measurements. For simplicity's sake, we will adopt the same nomenclature wherein hardness refers to microhardness or nanohardness. It should be noted that modulus values are sometimes reported as bulk modulus B and sometimes as nanoindentation modulus which is typically correlated with the Young's modulus E. The difference between E and B is normally small relative to the trends shown in the log-log plot of Figure 1. Therefore, the general term of modulus B is used throughout (see footnote in table 1 in Rakita et al.).[19]

Moduli values for $MAPbI_3$, $MAPbBr_3$ and $CsPbBr_3$ were taken from Rakita et al.[19] Values for the nanohardness of $MAPbX_3$ (X = Cl, Br, and I) were gathered from Sun et al.[21] and from Rakita et al.[19] for $CsPbBr_3$. Heat capacities for $MAPbX_3$ (X = Cl, Br, and I) were taken from Onoda–Yamamuro et al.[22] The heat capacity for $CsPbBr_3$ is taken from Haeger et al.[23] Thermal conductivity data came from Haeger et al.[23] for $CsPbBr_3$ and from Ge et al.[24] for $MAPbX_3$ (X = Cl, Br, and I).

From the plots in Figure 1a, it is clear that halides (and particularly lead HaPs) display low isothermal bulk modulus B and hardness H, which justifies categorizing them as "soft" materials, as is indeed frequently done. The low compliance of lead HaPs is well-known and -studied.[18,25] This behavior is attributed to the strong anharmonicity of the lattice potentials, with large fluctuations around the average lattice positions, as derived from diffraction data, of the halide ions compared to conventional semiconductors.[25] An empirical scaling law $B \propto \sqrt{H}$ is displayed as well in Figure 1a, fitting most materials except, most notably, Pb-HaPs. Instead, Pb-HaPs follow a scaling law of the form $B \propto 1/\sqrt{H}$, as discussed by Buchine et al.[26]

Regarding the thermal properties (Figure 1b), not only Pb-HaPs but also halides in general have low thermal conductivity and high linear thermal expansion coefficient. This phenomenon was previously identified by Ge et al.[24] on a smaller dataset, when comparing Pb-HaPs to other optoelectronic materials. The low thermal conductivity has been attributed to so called "rattling modes" of the methylammonium cations for $MAPbI_3$[27] and "cluster rattling modes" for Cs-based Pb-HaPs,[28,29] linked (once again) to the low bulk modulus and hardness. The mechanical softness and low compliance are well in line with the high linear thermal expansion coefficient, α, which points towards soft materials that show pronounced lattice expansion (or contraction) under thermal stimuli. The thermal conductivity, λ, is, though, unusually low for Pb-HaPs. This is expected, as those two thermal properties follow a scaling law $\alpha \propto 1/\sqrt{\lambda}$ that can be derived from thermodynamic considerations.[30,31]

Notably, those regions in the two diagrams, shown in Figure 1, occupied by halides and particularly by Pb-HaPs are well set off from the vast majority of the inorganic semiconductors. To test our hypothesis that materials with properties, similar to those of the Pb-HaPs on an Ashby diagram, will be good candidates for self-healing, we looked for semiconductors in those specific regions. A literature search revealed several such candidates, but none in terms of elastic modulus and hardness, where we included not only experimental and computed values, but also those from machine learning, in the MPDS database.

Several hits were obtained when the linear thermal expansion coefficient versus thermal conductivity data were searched. Results from the mostly experimental, peer-reviewed part of the MPDS are shown in Figure 1. These include AgBr within, and several others close to the phase space carved out by the HaPs, viz. $H_2(NH_4)(PO_4)$ (known as ADP), $LaCoO_3$ and CuI. Others are Cu_3SbS_3 and Cu_3SbSe_4. Those chalcogenides display low thermal conductivity, 0.4 and 1.3 $Wm^{-1}K^{-1}$, respectively, and a low hardness of 0.9 and 0.6 GPa, respectively.[32] Interestingly, the ultra-low thermal conductivity of these materials has been attributed to extreme anharmonicities of the lattice[33] and led them to be investigated as promising thermoelectrics.

Another candidate is the doped chalcogenide, p-type $Ag(Sb_{1-x}Zn_x)Te_2$. This material is also investigated for use as a thermoelectric, because of its ultralow thermal conductivity of 0.6 $Wm^{-1}K^{-1}$ at 300 K.[34] However, these doped semiconductors have a hardness in the range 2.5–6.5 GPa,[34] which is significantly higher than the threshold we identified earlier. At the same time, searching for SH in them will, in further work, allow testing our hypothesis about the required mechanical properties for SH. Because of the material's small bandgap, in the range 0.1–0.35 eV[35] also here mechanical or new types of SH studies will be needed, as this spectral range does not allow the use of FRAP.

More promising is a family of halide semiconductors for which reported values of the bulk elastic modulus are in the same range as those of the lead HaPs, the gold HaPs.[36,37] These compounds were first reported by Wells[38,39]; in recent years they received increased attention in theorical[40,41] and experimental[37,42,43] studies. They share the generic molecular formula $A_2Au^IAu^{III}X_6$ where A is a monovalent cation (Cs, Rb, or MA) and X a halide (Cl, Br, or I). They generally crystallize in a deformed perovskite structure, comprised of two different AuX_6 octahedra-like subunits for the different gold cations, Au^I and Au^{III}, and A cations occupying the lattice corners (**Figure 2**a). XPS measurements performed on these materials confirm the presence of the two gold valence states, Au^I and Au^{III},[44] an experiment that was successfully reproduced on our samples (Figure S4, Supporting Information).

We measured the indentation modulus on home-grown crystals of $Cs_2Au^IAu^{III}Br_6$ with both AFM, and INI (Instrumented Nano Indentation). The measurements yielded indentation modulus values of 16 GPa (± 3) GPa for INI and 14 (2) for AFM. Assuming a Poisson's ratio close to 0.3 as in lead HaPs,[19] the bulk and indentation moduli should be comparable.[19] Indeed, the measured values areclose to the bulk modulus value (13 Gpa) calculated previously for $Cs_2Au^IAu^{III}Cl_6$ from crystal constants.[36] It is also in the same range as the bulk moduli reported for lead HaPs.[19] The nanohardness, obtained from nano-indentation on the same sample, yielded a result of 0.79 GPa ± 0.14 GPa. This result firmly puts $Cs_2Au^IAu^{III}Br_6$ in the same region as the Pb-HaPs as shown in Figure 1a.

To investigate the self-healing properties of this family of materials, we used home-grown, continuous thin polycrystalline films of $Cs_2Au^IAu^{III}Cl_6$ and $Cs_2Au^IAu^{III}Br_6$ on FTO-covered glass slides. X-ray diffraction patterns from the obtained thin films, as discussed elsewhere, confirm that the material crystallizes in the deformed perovskite structure as previously mentioned.[38,39] The thin film patterns are in excellent agreement with those obtained from powders (A Py et al., TBP), with no additional peaks other than those associated with the FTO substrates. The presence of distinct coordination shells for gold ions is confirmed by the Raman spectrum (A Py et al., TBP), where each valence state is associated with a different feature, as discussed by Kojima.[45] The polycrystalline film results are in agreement with those obtained on powders, with the Au-associated peaks clearly visible around 300 and 325 cm^{-1}.

Figure 2b shows an SEM image of the surface morphology of a thin film of $Cs_2Au^IAu^{III}Cl_6$, confirming that the studied thin films are continuous with good coverage. Higher resolution images (Figure S5, Supporting Information) show that they consist of octahedral grains ranging in size from 200 to 500 nm. PL spectra of thin films of both the chloride and bromide compounds at room temperature are shown in Figure 2c.

Figure 3 shows the PL intensity change (decrease) upon damage, i.e., bleaching, and the subsequent recovery of the PL signal intensity as function of time after damage for unencapsulated thin films of $Cs_2Au^IAu^{III}Cl_6$ (Figure 3a) and $Cs_2Au^IAu^{III}Br_6$ (Figure 3b). The data points between $t = -100$ min and $t = 0$

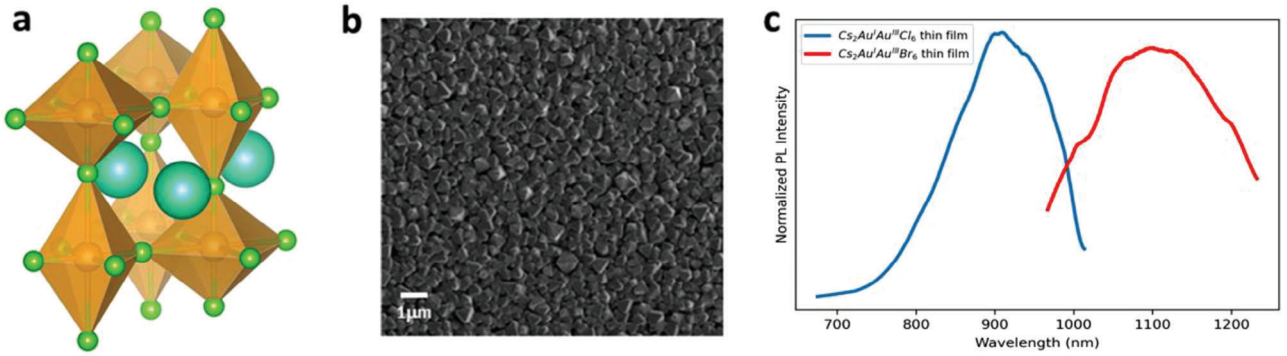

Figure 2. a) Schematic representation of $Cs_2Au^IAu^{III}X_6$ crystal structure with two octahedra of different size (Au^IX_6 and $Au^{III}X_6$). b) SEM SE image of the surface of a $Cs_2Au^IAu^{III}Cl_6$ thin film sample, showing a homogenous morphology of the fully converted film c) Room temperature PL spectra of $Cs_2Au^IAu^{III}Cl_6$ (CCD detector) and $Cs_2Au^IAu^{III}Br_6$ (InGaAs detector) thin films, uncorrected for the detector's response.

represent the PL intensity before bleaching. Samples are then exposed to orders of magnitude stronger illumination to induce damage, yielding the bleached state at $t = 0$, which manifests itself as a drop in photoluminescence intensity compared to the initial PL signal. Both $Cs_2Au^IAu^{III}Cl_6$ (Figure 3a) and $Cs_2Au^IAu^{III}Br_6$ (Figure 3b) exhibit a recovery of the PL intensity, similar to that observed in lead HaP thin films.[46]

We define the density of defects before photodamage as $[D] = [D]_b$. We then assume that the density of defects $[D]$, created during the initial photodamage, decays following the equation

$$[D] = [D]_{irr} + [D]_0 \, e^{-t/\tau} \tag{1}$$

where τ is defined as the characteristic lifetime of recovery, $[D]_{irr}$ the concentration of irreversible defects, i.e., defects that do not recover after the photodamage step, and $[D]_0$ the concentration of defects that self-heal. The PL intensity depends on the quenching of the PL signal by defects that function as recombination centers and shorten the non-radiative lifetime of the carriers, $\tau_{non\text{-}rad}$, an effect that can be modeled by the following relationship:

$$\tau_{non-rad} = C/[D] \tag{2}$$

where C is a constant. Furthermore, the non-radiative lifetime and the PL intensity, I_{PL}, are related by the following relationship:[47]

$$I_{PL} \propto \frac{1}{1 + (\tau_{rad}/\tau_{non-rad})} \tag{3}$$

where τ_{rad} is defined as the radiative recombination lifetime, and $\tau_{non\text{-}rad}$ the non-radiative recombination lifetime of carriers.[47]

It follows that before damage the PL intensity should follow the expression:

$$I_{PL}^{-1} \propto 1 + (\tau_{rad}/\tau_{non-rad}) \propto 1 + (\tau_{rad}[D]_b/C) \tag{4}$$

which is first order in t. After damage, this expression becomes:

$$I_{PL}^{-1} \propto 1 + \tau_{rad}/\tau_{non-rad} \propto 1 + (\tau_{rad}[D]_{irr}/C) + (\tau_{rad}[D]_0/C) \, e^{-t/\tau} \tag{5}$$

which remains first order in t. In analyzing the FRAP experiments we compare the ratio of PL intensities before and after photodamage. Hence, we study the evolution over time of the

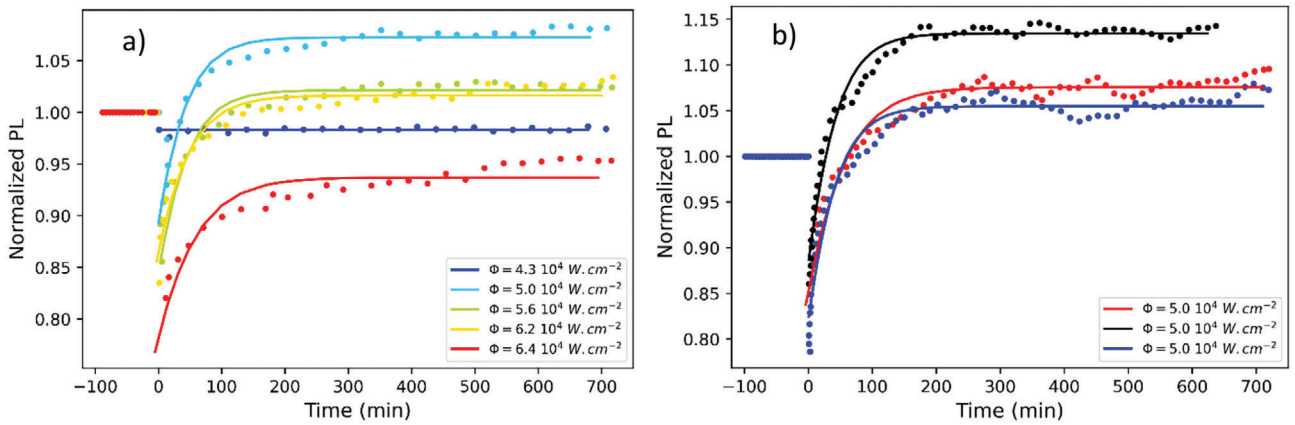

Figure 3. Photodamage and subsequent recovery dynamics of a) $Cs_2Au^IAu^{III}Cl_6$ and b) $Cs_2Au^IAu^{III}Br_6$ thin film during a FRAP experiment. The color-code for fluence of the photodamage for different curves is displayed on the graph. Dots represent experimental data of the PL intensity, normalized by the neighboring undamaged area, and solid lines are fits following Equation (5).

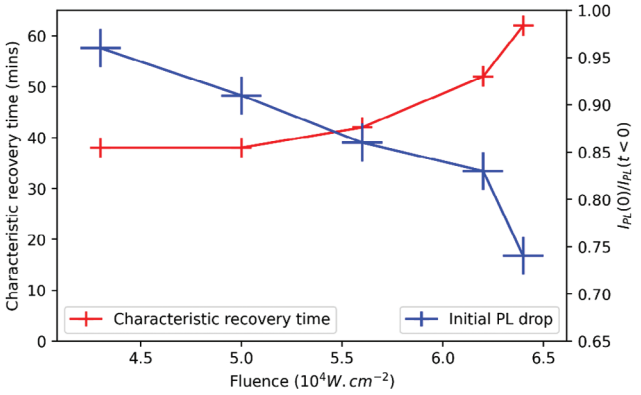

Figure 4. Characteristic recovery time (red) and initial drop in photoluminescence intensity (blue) versus fluence for a FRAP experiment on $Cs_2Au^IAu^{III}Cl_6$ thin films.

quantity $I_{PL}(t<0)$ / $I_{PL}(t)$. Based on the assumption that the density of defects follows Equation (1), we obtain

$$\frac{I_{PL}(t<0)}{I_{PL}(t)} \propto A + B\, e^{-t/\tau} \quad (6)$$

with A proportional to $\tau_{rad}/C \times [D]_b/[D]_{irr}$ and B proportional to $\tau_{rad}/C \times [D]_b/[D]_0$. The experimental data were fitted to Equation (5), and the fits are displayed as solid lines in Figure 3a for $Cs_2Au^IAu^{III}Cl_6$ and Figure 3b for $Cs_2Au^IAu^{III}Br_6$. The data are well represented by the proposed expression especially compared to expressions of the form $I_{PL} \propto t^a$, with R^2 values in the range 0.92–0.98 for all cases where recovery is observed. The initial PL intensity decrease, as well as the characteristic recovery time depend on the photon fluence exposure on the sample as is visible in **Figure 4**. The evolution of D_{irr} and D_0 with fluence in the case of a $Cs_2Au^IAu^{III}Cl_6$ thin film is discussed further in the Supporting Information.

The recovery times are comparable to those of $MAPbI_3$ and $FAPbI_3$[46] but significantly faster than for $CsPbBr_3$,[12] even though the studied thin films are also completely inorganic. On a longer timescale, the earlier noted increase in the intensity of the PL signal is seen for both Cs-Au-X film types.

The initial PL intensity decrease, as well as the characteristic recovery time depend on the photon fluence exposure on the $Cs_2Au^IAu^{III}Cl_6$ sample as is visible in Figure 4. It is furthermore observed that, generally at the lower fluences, the PL intensity after recovery can exceed the initial one (brightening), while at the higher fluences the sample may not fully recover, even after the longest times explored.

We ascribe this difference of PL intensity to defects that form as a result of the strong illumination (the damage) and which anneal out (i.e., self-heal), or to illumination-induced healing of pre-existing defects (yielding photo-brightening). Brightening after photodamage has been observed in some lead Pb-HaPs as well,[48] and can be attributed to a form of laser annealing.

Figure 5a displays the evolution of the PL spectrum of the $Cs_2Au^IAu^{III}Cl_6$ sample over time as measured, without correcting for the detector responsivity, showing the sharp decrease in intensity right after the laser damage, and, after 12 h, complete recovery to reach its previous intensity. Figure 5b displays those spectra, normalized to a common maximum, showing that the spectrum does not change in any significant manner during recovery. This excludes secondary phase formation as cause for the PL recovery and is, instead, consistent with self-healing of the luminescent phase.

A possible explanation for the evolution of the PL signal during the FRAP experiment is the creation and subsequent annihilation of point defects that influence the PL signal. Other explanations can be proposed to explain the PL changes, such as light-induced creation of secondary phases,[12] or photoinduced surface damage. The former is not likely in view of the formation energy of the gold halide perovskite from binaries, and would lead to changes in the emission spectrum. The latter cannot be completely discarded at this point, given that our PL recovery experiments were done on polycrystalline films with a high surface/volume ratio. As larger crystals become available, 2P-confocal PL microscopy will allow experimental testing of that explanation, by allowing a measurement representative of the bulk.

3. Conclusion

We presented a data-mining approach to meet the challenge of using Pb-HaPs to find other self-healing materials. Our hypothesis was that self-healing is a property that can be observed when several key features are simultaneously present in a material. To identify those, we scanned an experimental database for property combinations for which Pb- HaPs were exceptional compared to other semiconductors. This approach allowed us to identify specific areas, or target ranges, of these material property combinations, i.e., low thermal conductivity, combined with a high thermal expansion coefficient, low bulk modulus and small hardness, to search for candidate materials that can self-heal from damage. To test this hypothesis, we identified the family of compounds ($Cs_2Au^IAu^{III}X_6$, with X = I, Br, Cl) and prepared thin films and single crystals of $Cs_2Au^IAu^{III}Cl_6$ and $Cs_2Au^IAu^{III}Br_6$. We measured the mechanical properties of those crystals and found the nanohardness and indentation modulus to fit that of Pb-HaPs. We then measured the recovery of the photoluminescence signal after photo-damage on the thin films and found evidence for self-healing via photoluminescence recovery in these inorganic lead free HaPs, similar to what was found for Pb-HaPs. These findings show the power of data-mining in the quest for improved sustainability of materials, unlocking new search criteria of self-healing compounds.

4. Experimental Section

Synthesis of $Cs_2Au^iAu^{iii}Br_6$ Powders and Crystals: A 0.9 M CsBr solution was prepared in a mixed HBr (48%, Sigma): DI water (1:3) solution by stirring at room temperature for 2 h. 0.3 M $HAuCl_4$ (30 wt.% in dil. HCl, Sigma) was added to this solution slowly and under continuous stirring. Black precipitates of $Cs_2Au^IAu^{III}Br_6$ perovskite immediately form in the solution. The mixture was left to stir for an hour to ensure the completion of the reaction and then allowed to settle down the precipitates overnight. The solution was filtered, and the black precipitates were rinsed in water and ethanol, and then dried in a vacuum oven at 80 °C overnight. To measure the mechanical properties of the gold HaPs, as-synthesized powders were further used to grow single crystals using a low temperature antisolvent vapor saturation-based growth method. Briefly, a 1 M solution

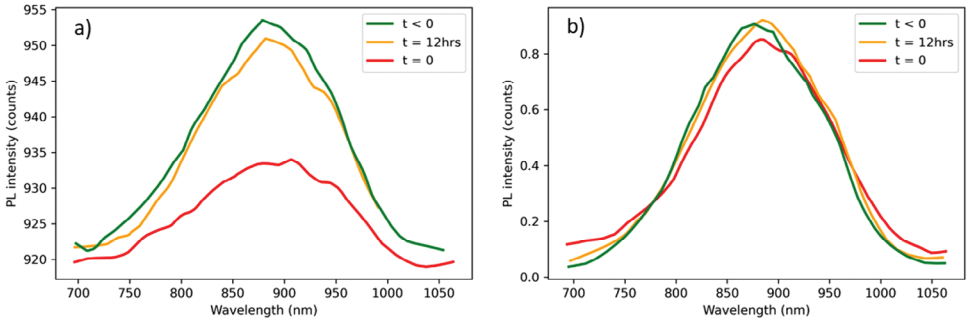

Figure 5. Photoluminescence spectra of an unencapsulated $Cs_2Au^IAu^{III}Cl_6$ thin film sample, a) Raw data and b) Normalized, before photodamage ($t < 0$), right after photodamage ($t = 0$) and after 12 h ($t = 12$ h) during a FRAP experiment.

$Cs_2Au^IAu^{III}Br_6$ was prepared in Dimethylformamide (DMF) solvent, filtered, and placed in a crystallization dish sealed with a suitable antisolvent. The details of the crystal synthesis and characterization were reported separately.

Growth of $Cs_2Au^IAu^{III}X_6$ Thin Films: A 400 nm FTO substrate (SOLEMS) was used for the preparation of thin films of the chosen semiconductor. A gold layer was deposited by electron beam evaporation (10^{-7} mbar base pressure) at an evaporation rate of 1 Å s^{-1}.

$Cs_2Au^IAu^{III}Cl_6$ thin films were prepared from a solution of HNO_3 in HCl (1: 3 v/v). 500 mg of CsCl was added to the solution, which was then spin-coated on top of the gold layer. CsCl and HCl were purchased from Alfa Aesar.

For $Cs_2Au^IAu^{III}Br_6$ thin film preparation, a solution of HNO_3 in HBr (47%) was prepared (1:3 v/v). 500 mg of CsBr was added to the solution. The resulting solution was then spin-coated on top of the gold layer. CsBr and HBr were purchased from Alfa Aesar.

Details of the film preparation, which yielded well-covering, continuous layers on the FTO substrate, and their in-depth film characterization results were published separately.

Self-Healing Experiment: The FRAP experiments were performed on an inverted optical microscope setup. Photodamage was performed with a continuous wave, blue (405 nm) laser (OBIS) using a 0.5 NA objective onto a diffraction-limited spot ($\sigma = 1.2$ µm), where the laser irradiated each spot on the film with varying power densities. Following photodamage, the damaged region of the sample was illuminated by a blue (405 nm) LED (Mightex) and fluorescence emitted from the sample was epi-detected and imaged onto an EMCCD detector (Andox Ixon Ultra 897). To track the time evolution of the PL spectra for each of the damaged spots, low (not damaging) laser power was used, and the PL was directed to a spectrometer (ANDOR Shamrock SR-303i).

Mechanical Measurements on Single Crystals: The nanomechanical measurements were performed using both instrumented nanoindentation, (INI), and Peak Force Quantitative Nanomechanical Measurements (PF-QNM). INI was performed in a KLA-Tencor XP nanoindenter using a Berkovich indenter tip and continuous stiffness measurement (CSM), which gives continuous values of hardness (H) and indentation modulus (E) as a function of depth. Indentations were made to a depth of 1 µm, although the E values overcame surface effects and leveled off after 200–250 nm. The values reported were average over 650–900 nm depth. PF-QNM measurements were made on a Multimode AFM (Bruker) with dedicated software for performing and analyzing the data. A pre-calibrated probe, RTESP-525-30 (Bruker) was used for the measurements. Measurements were made over a surface area of (1 μm^2), with 96 × 96 pixels: the modulus was calculated at each pixel and average values + standard deviations were reported. Typical curves of INI Hardness and Modulus versus Displacement into the surface were shown in Figure S1(Supporting Information).

Data-Mining Methodology: The Material Platform was used for Data Science (MPDS) database[49] for data-mining. The data set was probed with the database's dedicated Application Programming Interface (API). To highlight the overall trends from a discrete set of data points, kernel density estimates were used.[50,51]

All of the data considered, except where noted for the Cs-Au-halides, were published in peer-reviewed journals.[52]

To identify which properties were relevant for this study, the selected 30 material properties and based on the number of entries (properties with <100 entries were discarded, see Table S1, Supporting Information), further restricted study to 17 material properties across the MPDS database. For a better visual representation the distribution of values were plotted across the database for different properties in the form of so-called Ashby diagrams,[53] 2D plots each showing correlation between two different physical properties.

Supporting Information

Supporting Information is available from the Wiley Online Library or from the author.

Acknowledgements

Omer Yaffe for fruitful discussions. A.P.R., P.S., J.F.G., P.S., S.K., and D.C. gratefully acknowledge support from a Weizmann-CNRS grant and thank Omer Yaffe for fruitful discussions. D.C. thanks Igor Lubomirsky for a seminal early discussion. A.P.R., P.S., and J.F.G. gratefully acknowledge the support of the IPVF technological platform. D.O. and D.C. gratefully acknowledge financial support from the Weizmann Sustainability and Energy Research Initiative, SAERI. D.C. and P.S. thank the Minerva Centre for Self-Repairing Systems for Energy & Sustainability and the Helen and Martin Kimmel Center for Nanoscale Science for support. Y.S. was supported by the Ariane de Rothschild Women Doctoral Program. D.R.C. thanks the European Union's Horizon 2020 research & innovation program under a Marie Sklodowska-Curie grant agreement, No. 893194. D.O. is the incumbent of the Harry Weinrebe Professorial Chair of laser physics.

Conflict of Interest

The authors declare no conflict of interest.

Author Contributions

A.P.R. performed film synthesis, data curation, formal analysis, defect model (with J.F.G. and D.R.C.), investigation, visualization, and writing. J.F.G. performed conceptualization of the project, formal analysis, funding acquisition (with P.Sc.), investigation, methodology (thin film preparation, PL analysis), supervision, and validation. P.Sc. performed conception

of the project, funding acquisition, methodology (materials and sample preparation, characterization, supervision, and writing. D.C. performed statement of the problem, concept, planning, overseeing, writing, and funding (with D.O.). D.O. and S.H. performed experiment and data analysis supervision, writing, and funding. P.Si. andY.S. . performed experiments and data analyses. S.C. and I.R.G. performed AFM. and nanoindentation experiments and data analyses. S.K. performed single crystal growth, mechanical measurements, and data analyses.

Data Availability Statement

The data that support the findings of this study are available from Materials Platform for Data Science. Restrictions apply to the availability of these data, which were used under license for this study. Data are available from the authors with the permission of Materials Platform for Data Science.

Keywords

self-healing, thin films, photovoltaic, data mining, gold halide perovoskites

Received: August 30, 2023
Revised: September 21, 2023
Published online:

[1] M. A. Green, E. D. Dunlop, G. Siefer, M. Yoshita, N. Kopidakis, K. Bothe, X. Hao, *Prog. Photovoltaics Res. Appl.* **2023**, *31*, 3.
[2] Z. Zhang, H. Wang, T. J. Jacobsson, J. Luo, *Nat. Commun.* **2022**, *13*, 7639.
[3] Y. Guo, O. Yaffe, T. D. Hull, J. S. Owen, D. R. Reichman, L. E. Brus, *arXiv* **2018**.
[4] D. A. Egger, A. Bera, D. Cahen, G. Hodes, T. Kirchartz, L. Kronik, R. Lovrincic, A. M. Rappe, D. R. Reichman, O. Yaffe, *Adv. Mater.* **2018**, *30*, 1800691.
[5] S. Kumar, G. Hodes, D. Cahen, *MRS Bull.* **2020**, *45*, 478.
[6] R. E. Brandt, V. Stevanovic, D. S. Ginley, T. Buonassisi, *MRS Commun.* **2015**, *5*, 265.
[7] D. Cahen, L. Kronik, G. Hodes, *ACS Energy Lett.* **2021**, *6*, 4108.
[8] J.-F. Guillemoles, U. Rau, L. Kronik, H.-W. Schock, D. Cahen, *Adv. Mater.* **1999**, *11*, 957.
[9] J. J. Wysocki, *IEEE Trans. Nucl. Sci.* **1966**, *13*, 168.
[10] I. Lyubomirsky, V. Lyakhovitskaya, J. F. Guillemoles, I. Riess, R. Triboulet, D. Cahen, *J. Cryst. Growth* **1996**, *161*, 90.
[11] I. Lyubomirsky, V. Lyakhovitskaya, R. Triboulet, D. Cahen, *Appl. Phys. Lett.* **1995**, *67*, 3132.
[12] D. R. Ceratti, Y. Rakita, L. Cremonesi, R. Tenne, V. Kalchenko, M. Elbaum, D. Oron, M. A. C. Potenza, G. Hodes, D. Cahen, *Adv. Mater.* **2018**, *30*, 1706273.
[13] D. R. Ceratti, A. V. Cohen, R. Tenne, Y. Rakita, L. Snarski, N. P. Jasti, L. Cremonesi, R. Cohen, M. Weitman, I. Rosenhek-Goldian, I. Kaplan-Ashiri, T. Bendikov, V. Kalchenko, M. Elbaum, M. A. C. Potenza, L. Kronik, G. Hodes, D. Cahen, *Mater. Horiz.* **2021**, *8*, 1570.
[14] A. V. Cohen, D. A. Egger, A. M. Rappe, L. Kronik, *J. Phys. Chem. Lett.* **2019**, *10*, 4490.
[15] S. K. Yadavalli, Z. Dai, H. Zhou, Y. Zhou, N. P. Padture, *Acta Mater.* **2020**, *187*, 112.
[16] M. B. Al-Handawi, G. Dushaq, P. Commins, D. P. Karothu, M. Rasras, L. Catalano, P. Naumov, *Adv. Mater.* **2022**, *34*, 2109374.
[17] M. J. Schilcher, P. J. Robinson, D. J. Abramovitch, L. Z. Tan, A. M. Rappe, D. R. Reichman, D. A. Egger, *ACS Energy Lett.* **2021**, *6*, 2162.
[18] A. C. Ferreira, A. Létoublon, S. Paofai, S. Raymond, C. Ecolivet, B. Rufflé, S. Cordier, C. Katan, M. I. Saidaminov, A. A. Zhumekenov, O. M. Bakr, J. Even, P. Bourges, *Phys. Rev. Lett.* **2018**, *121*, 085502.
[19] Y. Rakita, S. R. Cohen, N. K. Kedem, G. Hodes, D. Cahen, *MRS Commun.* **2015**, *5*, 623.
[20] G. A. Elbaz, W.-L. Ong, E. A. Doud, P. Kim, D. W. Paley, X. Roy, J. A. Malen, *Nano Lett.* **2017**, *17*, 5734.
[21] S. Sun, Y. Fang, G. Kieslich, T. J. White, A. K. Cheetham, *J. Mater. Chem. A* **2015**, *3*, 18450.
[22] N. Onoda-Yamamuro, T. Matsuo, H. Suga, *J. Phys. Chem. Solids* **1990**, *51*, 1383.
[23] T. Haeger, M. Wilmes, R. Heiderhoff, T. Riedl, *J. Phys. Chem. Lett.* **2019**, *10*, 3019.
[24] C. Ge, M. Hu, P. Wu, Q. Tan, Z. Chen, Y. Wang, J. Shi, J. Feng, *J. Phys. Chem. C* **2018**, *122*, 15973.
[25] C. Katan, A. D. Mohite, J. Even, *Nat. Mater.* **2018**, *17*, 377.
[26] I. Buchine, I. Rosenhek-Goldian, N. P. Jasti, D. R. Ceratti, S. Kumar, D. Cahen, S. R. Cohen, *Commun. Mater.* **2022**, *3*, 70.
[27] T. Hata, G. Giorgi, K. Yamashita, *Nano Lett.* **2016**, *16*, 2749.
[28] W. Lee, H. Li, A. B. Wong, D. Zhang, M. Lai, Y. Yu, Q. Kong, E. Lin, J. J. Urban, J. C. Grossman, P. Yang, *Proc. Natl. Acad. Sci* **2017**, *114*, 8693.
[29] S. Kawano, T. Tadano, S. Iikubo, *J. Phys. Chem. C* **2021**, *125*, 91.
[30] C. L. Julian, *Phys. Rev.* **1965**, *137*, A128.
[31] G. Grimvall, in *Thermophysical Properties of Materials*, Elsevier, USA, pp. 200, **1999**.
[32] K. Tyagi, B. Gahtori, S. Bathula, V. Toutam, S. Sharma, N. K. Singh, A. Dhar, *Appl. Phys. Lett.* **2014**, *105*, 261902.
[33] Y. Zhang, E. Skoug, J. Cain, V. Ozolins, D. Morelli, C. Wolverton, *Phys. Rev. B* **2012**, *85*, 054306.
[34] S. Roychowdhury, R. Panigrahi, S. Perumal, K. Biswas, *ACS Energy Lett.* **2017**, *2*, 349.
[35] K. Hoang, S. D. Mahanti, J. R. Salvador, M. G. Kanatzidis, *Phys. Rev. Lett.* **2007**, *99*, 156403.
[36] N. Matsushita, H. Ahsbahs, S. S. Hafner, N. Kojima, *J. Solid State Chem.* **2007**, *180*, 1353.
[37] B. Bajorowicz, A. Mikolajczyk, H. P. Pinto, M. Miodynska, W. Lisowski, T. Klimczuk, I. Kaplan-Ashiri, M. Kazes, D. Oron, A. Zaleska-Medynska, *J. Phys. Chem. C* **2020**, *124*, 26769.
[38] H. L. Wells, *Am. J. Sci.* **1922**, *s5-4*, 476.
[39] H. L. Wells, *Am. J. Sci.* **1922**, *s5-3*, 315.
[40] L. Debbichi, S. Lee, H. Cho, A. M. Rappe, K.-H. Hong, M. S. Jang, H. Kim, *Adv. Mater.* **2018**, *30*, 1707001.
[41] J. Kangsabanik, S. Ghorui, M. Aslam, A. Alam, *Phys. Rev. Appl.* **2019**, *13*, 014005.
[42] H. Murasugi, S. Kumagai, H. Iguchi, M. Yamashita, S. Takaishi, *Chem. – A Eur. J.* **2019**, *25*, 9885.
[43] B. Ghosh, B. Febriansyah, P. C. Harikesh, T. M. Koh, S. Hadke, L. H. Wong, J. England, S. G. Mhaisalkar, N. Mathews, *Chem. Mater.* **2020**, *32*, 6318.
[44] J.-Y. Son, T. Mizokawa, J. W. Quilty, K. Takubo, K. Ikeda, N. Kojima, *Phys. Rev. B – Condens. Matter Mater. Phys.* **2005**, *72*, 4.
[45] N. Kojima, *Bull. Chem. Soc. Jpn.* **2000**, *73*, 1445.
[46] P. Singh, Y. Soffer, D. R. Ceratti, M. Elbaum, D. Oron, G. Hodes, D. Cahen, *Submitt. under Revis.* **2023**.
[47] M. Leroux, N. Grandjean, B. Beaumont, G. Nataf, F. Semond, J. Massies, P. Gibart, *J. Appl. Phys.* **1999**, *86*, 3721.
[48] W.-A. Quitsch, D. W. Dequilettes, O. Pfingsten, A. Schmitz, S. Ognjanovic, S. Jariwala, S. Koch, M. Winterer, D. S. Ginger, G. Bacher, *J. Phys. Chem. Lett.* **2018**, *9*, 2062.
[49] E. Blokhin, P. Villars, C. Karin, O. Hiro, MPDS: Materials Platform for Data Science, https://www.researchgate.net/project/Materials-Platform-for-Data-Science, **2017**.
[50] E. Parzen, *Ann. Math. Stat.* **1962**, *33*, 1065.
[51] M. Rosenblatt, *Ann. Math. Stat.* **1956**, *27*, 832.
[52] E. Blokhin, P. Villars, in *Handb. Mater. Model.* (Eds.: W. Andreoni, S. Yip), Springer, Cham pp. 1–25, **2019**.
[53] M. F. Ashby, *Mater. Sel. in Mech. Des.*, Elsevier, USA, pp. 57, **2011**.